Available online at www.sciencedirect.com
ScienceDirect
Journal of Asian Earth Sciences 29 (2007) 490–503
Journal of Asian Earth Sciences
www.elsevier.com/locate/jaes

Geometric evolution of a plate interface–branch fault system: Its effects on the tectonic development of the Himalayas

Youichiro Takada [a,*], Mitsuhiro Matsu'ura [b]

[a] Division of Earth and Planetary Sciences, Hokkaido University, Sapporo 060-0810, Japan
[b] Department of Earth and Planetary Science, University of Tokyo, Tokyo 113-0033, Japan

Received 11 February 2005; accepted 11 October 2005

Abstract

Crustal deformation due to fault slip depends strongly on fault geometry, and fault geometry is changed by the deformation of the crust. This feedback mechanism causes the geometrical evolution of the fault system. We have studied the progress of the geometrical evolution of a plate interface–branch fault system through numerical simulation, based on elastic–viscoelastic dislocation theory. If the plate interface is smooth, no significant change occurs in fault geometry. If the plate interface has a ramp, we observe the gradual horizontal motion of the ramp toward the hanging-wall side of the interface at half the plate convergence rate. The offset of the ramp decreases with time. The dip-angle of thrust faults branching from the plate interface increases more rapidly as the dip of the fault increases. We have applied these results to the plate interface–branch fault system at the India–Eurasia collision boundary and obtained a scenario for the tectonic development of the Himalayas for the last 30 Myr.

Keywords: Himalaya; geometric evolution; ramp; branch fault; dislocation theory

1. Introduction

According to Molnar and Tapponnier (1975), the collision between India and Eurasia began at the Indus suture zone in early Tertiary time. Subsequently, at about 30 Myr BP, the collision boundary shifted southward. The Himalayas have been developed since then. Fig. 1 shows the present tectonic setting of the India–Eurasia collision zone. The convergence rate between the Indian and the Eurasian plates has been estimated as about 50 mm/yr (DeMets et al., 1990). At the collision boundary extending along the Himalayas, about 40% of the total convergence rate is consumed by the subduction of the Indian Plate beneath the Eurasian Plate (e.g. Lyon-Caen and Molnar, 1985; Bilham et al., 1997). The remaining 60% is consumed by internal deformation of the Eurasian Plate (e.g. England and Molnar, 1997).

A number of geodetic and geologic observations indicate that the India–Eurasia plate interface includes a large-scale ramp beneath the High Himalaya (e.g. Kono, 1974; Schelling and Arita, 1991). As shown in Fig. 2, the shallower part of the plate interface is accompanied by a series of large-scale branching thrust faults, the Main Central Thrust (MCT), the Main Boundary Thrust (MBT) and the Main Frontal Thrust (MFT). In the Himalaya rapid crustal uplift due to the India–Eurasia collision continues at present (e.g. Iwata et al., 1984; Jackson and Bilham, 1994). Many theoretical studies indicate that the present pattern of crustal deformation depends strongly on the geometry of the plate interface–branch fault system (e.g. Molnar, 1987; Jackson and Bilham, 1994; Takada and Matsu'ura, 2004). The geometry of a fault system changes on a geologic time-scale because of cumulative crustal deformation due to seismic and/or aseismic fault motion. Therefore, to understand the process of tectonic develop-

* Corresponding author. Address: Department of Earth Sciences, University of Oxford, Parks Road, OX1 3PR Oxford, UK Tel.: +44 1865 272 068; fax: +44 1865 272 072.
E-mail address: yopan@earth.ox.ac.uk (Y. Takada).

1367-9120/$ - see front matter
doi:10.1016/j.jseaes.2005.10.013

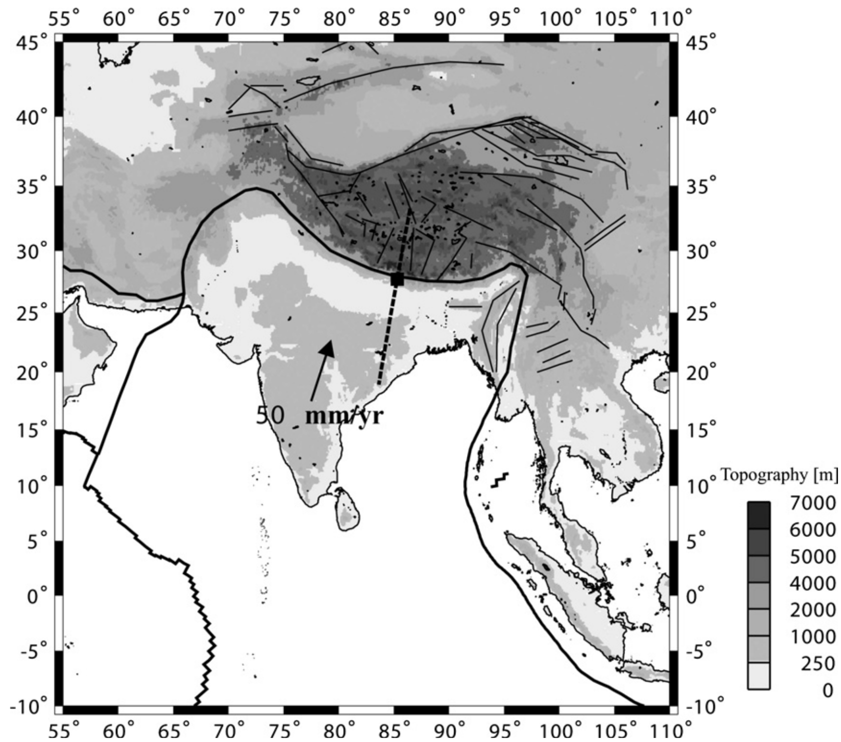

Fig. 1. Present tectonic setting of the India–Eurasia collision zone. The thick solid lines represent plate boundaries. The arrow indicates the velocity vector of India relative to Eurasia, calculated from NUVEL-1 (DeMets et al., 1990). The thin lines indicate active faults (England and Molnar, 1997). The thick broken line indicates a reference line crossing the collision boundary at Kathmandu (the solid square).

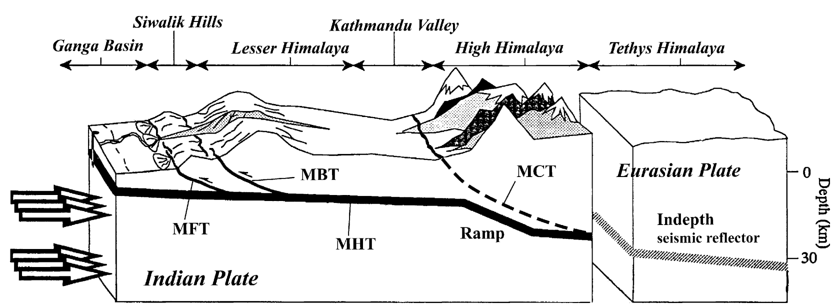

Fig. 2. A schematic diagram showing the plate interface–branch fault system in Himalaya (modified from Jackson and Bilham, 1994). MFT, Main Frontal Thrust; MBT, Main Boundary Thrust; MCT, Main Central Thrust; MHT, Main Himalayan Thrust.

ment in the Himalaya, we should consider the effects of the long term geometrical evolution of the plate interface–branch fault system.

On the basis of geological and geophysical evidence Lyon-Caen and Molnar (1983) and Harrison et al. (1992), for example, have reconstructed the past history of tectonic development in the Himalaya by considering the effects of geometrical evolution of the fault system. However, in these studies the mechanism of the geometrical evolution of the fault system is unclear. Therefore, it is necessary to clarify the physical feedback mechanism governing the process of geometrical evolution of the plate interface–branch fault system.

Physical models have been proposed previously for the topographic development of collisional mountains. Davis et al. (1983) have modelled the fold-and-thrust belt as a critically tapered wedge of (Coulomb wedge). This model is only applicable to the frontal part of collisional mountains. Willett et al. (1993) have proposed a model of topographic development in which the steady convergence of two rigid plates deforms an overlying rigid-plastic surface layer. Using this model they reproduced the characteristic pattern of branch thrusts commonly observed in the frontal part of collisional mountains. Chemenda and his co-workers (Shemenda and Grocholsky, 1992; Chemenda et al., 1995, 1996, 2000) have investigated the process of the tectonic development of collisional mountains by using an analogue model consisting of brittle and ductile clay layers. The main purpose of these analogue experiments was to understand very large-scale geometric evolution of the Indian slab. Thus, little attention has been directed to the effects of the geometrical evolution of the plate interface–branch fault system on the tectonic development of collisional mountains.

Mechanical interaction at a plate interface can be represented naturally by an increase in the tangential displacement discontinuity (dislocation) across the plate interface (Matsu'ura and Sato, 1989). On this basis Sato and Matsu'ura (1993) have developed a long-term plate subduction model and have succeeded in explaining the whole process of formation of island arc-trench systems. Recently, Takada and Matsu'ura (2004) have demonstrated that the present vertical movement in Himalaya and horizontal deformation in Tibet can be explained by a single plate-convergence model.

The purpose of the present study is to reveal the physical feedback mechanism governing the process of geometrical evolution of the plate interface–branch fault system. In Section 2, we summarize briefly the observations of the plate interface–branch fault system in the Himalaya. In Section 3, first we construct a kinematic model for plate convergence on the basis of elastic–viscoelastic dislocation theory and then compute the internal deformation field in the Himalaya due to the steady under-thrusting of the Indian Plate. In Section 4, by incorporating a feedback algorithm for the change of fault geometry into the kinematic plate convergence model, we numerically simulate the geometrical evolution processes of the plate interface–branch fault system and the corresponding surface uplift pattern. In Section 5, by combining the numerical results of the evolution of the geometrical fault-system with geological knowledge, we propose a scenario for the tectonic development of the Himalayas over the last 30 Myr.

2. The plate interface–branch fault system in Himalaya

First of all, we summarize briefly the observational data concerning the geometry of the India–Eurasia plate interface in the Himalaya, the Main Himalayan Thrust (MHT), and its long-term slip rates. Jackson and Bilham (1994) have deduced the plate interface geometry in Nepal from the analysis of various kinds of data. The project INDEPTH has revealed the plate interface geometry in the southern part of Tibet by seismic reflection profiling (Zhao et al., 1993; Nelson et al., 1996; Brown et al., 1996). From these comprehensive studies we can extract the following geometrical features of the plate interface. The plate interface dips gently beneath the Lesser Himalaya and the southern part of Tibet, but steepens abruptly beneath the High Himalaya. Thus, the plate interface has a ramp structure beneath the High Himalaya. Bouguer gravity anomalies (e.g. Kono, 1974; Lyon-Caen and Molnar, 1983), fault plane solutions of moderate-size earthquakes (Ni and Barazangi, 1984; Baranowski et al., 1984), and balanced cross sections (Schelling and Arita, 1991; Schelling, 1992) consistently indicate the presence of a ramp structure beneath the High Himalaya. From the ages of sediments in drill holes in the Ganga Basin, Lyon-Caen and Molnar (1985) estimated the slip rate at the plate interface to average 15±5 mm/yr, over the last 15–20 Myr. On the other hand, from the inversion analysis of GPS data, Bilham et al. (1997) and Larson et al. (1999) obtained slip rates of 20.5±5 and 20±1 mm/yr, respectively, for the deeper part of the plate interface.

Next, we review the past slip-history and the present geometry of the major thrust faults branching from the plate interface. In the history of the tectonic development of the Himalaya the first major event is the formation of the Main Central Thrust (MCT). The High Himalaya with the peak altitude of about 8000 m is bounded to the south by the MCT (Fig. 2). In this region, there are Tertiary two-mica granitic intrusions, which can be regarded as evidence of thrust motion along the MCT. Through the compilation of data from these granites by Molnar (1984), Hodges et al. (1988) and Harrison et al. (1992), it has been confirmed that the age of intrusion ranges widely from Upper Oligocene to Middle Miocene. Thus, the age of the initiation of thrust motion on the MCT is generally assumed to be about 30 Myr BP (e.g. Harrison et al., 1992). Another constraint on the slip history is obtained from inverted metamorphism around the MCT, caused by thrust motion on the MCT. The age of inverted metamorphism has been estimated as about 15–20 Myr BP (e.g. LeFort, 1986). On the basis of these observations we can estimate that the active phase of the MCT was from 30 to 15 Myr BP. From balanced cross-sections Schelling and Arita (1991) and Schelling (1992) have estimated the total convergence accommodated by the MCT for this period to be 140–210 km. From changes in the dip-angle of the surface rocks, many geologists (e.g. Gansser, 1964; Schelling and Arita, 1991; Schelling, 1992) have inferred that the MCT dips steeply near the surface but more gently at depth, as illustrated in Fig. 2.

Another large-scale branch fault, the Main Boundary Thrust (MBT), lies to the south of the MCT. The MBT runs along the southern foot of the Lesser Himalaya at an altitude of about 2000 m. The age of the initiation of thrust motion along the MBT is estimated to be latest Miocene or Pliocene, based on a sudden increase in sedimentation rates, fission track dating of the hanging-wall rocks, and balanced cross-sections (e.g. Gansser, 1981; Meigs et al., 1995; DeCelles et al., 2001). Although the precise age is still unknown, it is widely accepted that the activity of the MBT started later than the cessation of activity of the MCT. Nakata et al. (1990) and Mugnier et al. (1994) have shown that recent thrust motion on the MBT is not continuous along the strike of the fault. Thus, we may conclude that thrust motion at the MBT will soon cease over the whole fault. From a balanced cross-section Schelling (1992) has estimated that the total convergence accommodated by the MBT is about 45 km. From surface geology and balanced cross-sections, many geologists (e.g. Gansser, 1964; Schelling and Arita, 1991; Schelling, 1992; Mugnier et al., 1994) have inferred that the MBT has also a listric shape, with a very steep dip-angle at the surface.

The Main Frontal Thrust (MFT) is the youngest thrust fault branching from the MHT. From river terrace data Wesnousky et al. (1999) and Lavé and Avouac (2000) have estimated that the present slip rate at the MFT is about 14 and 21 mm/yr, respectively. The Siwalik Hills, which mark the deformation front of the Himalayas, have been produced by activity along the MFT. There is no geologic evidence that directly indicates the age of the initiation of thrust motion along the MFT, but the age of initiation is usually assumed to be Pliocene–Holocene (Molnar, 1984; Hodges, 2000). From balanced cross-sections Schelling (1992) and Powers et al. (1998) have estimated the total convergence accommodated by the MFT and minor faults to the south of the MBT to be about 25 km. From balanced cross-sections and seismic exploration, many geologists (Schelling and Arita, 1991; Schelling, 1992; Friedenreich et al., 1994) have shown that the MFT also has a listric shape.

3. A plate convergence model and internal deformation fields

3.1. Development of a kinematic plate convergence model

In this subsection, we develop a kinematic model for plate convergence on the basis of elastic–viscoelastic dislocation theory (Matsu'ura and Sato, 1989). First, we model the lithosphere–asthenosphere system by a two-layered half-space, consisting of an elastic surface layer and a viscoelastic substratum, under the influence of gravity. Here, the elastic surface layer and the viscoelastic substratum correspond to the lithosphere and the asthenosphere, respectively. Analyses of post-glacial uplift data show that the lithosphere and the asthenosphere behave like a perfectly elastic solid and a Maxwell fluid with the viscosity of 10^{19}–10^{20} Pa s on a time-scale shorter than 10^6 yr (Cathles, 1975; Iwasaki and Matsu'ura, 1982). In tectonically active regions such as the India–Eurasia collision zone, the viscosity of the asthenosphere has a somewhat smaller value (5×10^{18} Pa s) than this global average. In the present study, we treat crustal deformation on the time-scale of 10^4–10^7 yr. On the time-scale of 10^7 yr, as demonstrated by Sato and Matsu'ura (1993) and Takada and Matsu'ura (2004), the viscoelastic stress relaxation of the lithosphere decreases the deformation rate, but does not change the deformation pattern significantly. Therefore, considering these effects, for simplicity we may represent the rheology of the lithosphere as purely elastic. The constitutive equation of the elastic surface layer can be written as:

$$\begin{cases} \sigma_{kk} = 3\kappa_1\varepsilon_{kk} \\ \sigma'_{ij} = 2\mu_1\varepsilon'_{ij} \end{cases} \tag{1}$$

and that of the Maxwellian viscoelastic substratum as:

$$\begin{cases} \sigma_{kk} = 3\kappa_2\varepsilon_{kk} \\ \dot{\sigma}'_{ij} + \frac{\mu_2}{\eta}\sigma'_{ij} = 2\mu_2\dot{\varepsilon}'_{ij} \end{cases} \tag{2}$$

where σ_{ij} and ε_{ij} are the stress and strain tensors, σ'_{ij} and ε'_{ij} are the deviatoric stress and strain tensors. The constants μ_i and κ_i ($i = 1,2$) denote the shear modulus and the bulk modulus of the i-th layer, and η represents the viscosity of the second layer (substratum). The dot indicates differentiation with respect to time. The constitutive Eq. (2) states that the viscoelastic substratum behaves like a Maxwell fluid in shear and an elastic solid in bulk.

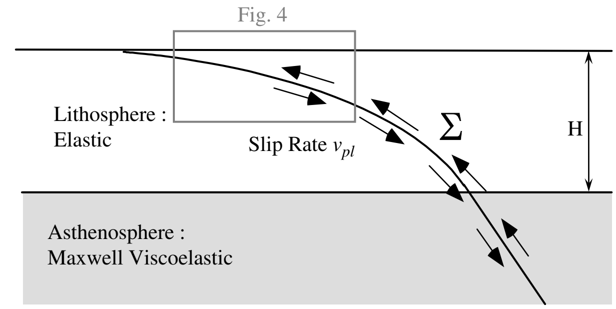

Fig. 3. Schematic representation of a kinematic plate convergence model. Mechanical interaction at the plate interface Σ is represented by tangential displacement discontinuity at the increase rate of v_{pl}. The structure model consists of an elastic surface layer with a thickness H and a viscoelastic substratum, which correspond to the lithosphere and the asthenosphere, respectively.

Next, we introduce an interface Σ that divides the stratified elastic–viscoelastic half-space into two blocks, the Eurasian and the Indian blocks, as shown in Fig. 3. The steady increase of the tangential displacement discontinuity across the interface Σ represents the steady subduction of the Indian Plate. Here, it should be noted that the tangential displacement discontinuity is mathematically equivalent to the force system of a double couple (Maruyama, 1963; Burridge and Knopoff, 1964), which brings about crustal deformation. In general, the force system acting on the plate interface must have the properties of no net force and no net torque, since it is the internal force imposed by a dynamic process within the Earth. The double couple force system always satisfies the above conditions. This is one of the reasons why we represent mechanical interaction at plate interfaces by the increase of tangential displacement discontinuity. Another reason is more practical; the geometry and slip rates of plate interfaces can be directly estimated from geophysical and geodetical observations.

The boundary conditions in the present problem are no traction at the surface of the half-space, continuity of displacement and traction across the lithosphere–asthenosphere boundary, and uniform slip at a constant rate on the whole plate interface Σ. The surface boundary conditions are always defined on a flat plane (depth = 0 km).

Finally, we present the mathematical formulations required for the calculation of crustal deformation due to steady plate subduction. The viscoelastic displacement fields $\mathbf{u}(\mathbf{x},t)$ due to arbitrary slip motion on the plate interface Σ are generally given by the following hereditary integral:

$$\mathbf{u}(\mathbf{x},t) = \int_{-\infty}^{t}\int_{\Sigma}\left[\frac{\mathrm{d}f_s(\tau)}{\mathrm{d}\tau}\right]\mathbf{q}(\mathbf{x},t;\mathbf{x}',\tau)\mathrm{d}\mathbf{x}'\mathrm{d}\tau. \tag{3}$$

here, $\mathbf{q}(\mathbf{x},t;\mathbf{x}',\tau)$ denotes the displacement at an arbitrary point $\mathbf{x}$ and a time t caused by a unit step slip at a point $\mathbf{x}'$ on Σ at a time τ, and f_s is a slip time function. Assuming the steady slip on Σ starts at $t = 0$, we may write the slip time function as:

$$f_s = v_{pl} t H(t) \tag{4}$$

where $H(t)$ denotes the unit step function and v_{pl} is the plate convergence rate. Assuming the plate convergence rate v_{pl} to be constant, we can rewrite Eq. (3) as:

$$\mathbf{u}(\mathbf{x}, t) = v_{pl} \int_o^t \int_\Sigma \mathbf{q}(\mathbf{x}, t; \mathbf{x}', \tau) \mathrm{d}\mathbf{x}' \mathrm{d}\tau. \tag{5}$$

The displacement rates due to steady plate subduction are given by the time derivatives of Eq. (5) as:

$$\dot{\mathbf{u}}(\mathbf{x}, t) \equiv \frac{\partial \mathbf{u}(\mathbf{x}, t)}{\partial t} = v_{pl} \int_\Sigma \mathbf{q}(\mathbf{x}, t; \mathbf{x}', 0)\, \mathrm{d}\mathbf{x}'. \tag{6}$$

In this description the time dependence of displacement rates comes from only the stress relaxation in the asthenosphere. As demonstrated by Sato and Matsu'ura (1993) and Takada and Matsu'ura (2004), the characteristic relaxation time of the asthenosphere is of the order of 10–10^2 years. Since the time-scale of the present problem is much longer than the characteristic relaxation time of the asthenosphere, we may consider the case of $t = \infty$ in practice. Accordingly, Eq. (6) can be simplified as:

$$\mathbf{u}(\mathbf{x}, t) = v_{pl} \int_\Sigma \mathbf{q}(\mathbf{x}, \infty; \mathbf{x}', 0)\, \mathrm{d}\mathbf{x}'. \tag{7}$$

The above equation states that the displacement rates due to steady plate subduction are simply given by the integration of the viscoelastic step responses $\mathbf{q}$ at $t = \infty$ over the whole plate interface Σ.

The viscoelastic response to a unit step slip $\mathbf{q}(\mathbf{x},t;\mathbf{x}',\tau)$ can be derived from the solution of the associated elastic problem (Sato and Matsu'ura, 1973; Fukahata and Matsu'ura, 2005) by applying the correspondence principle of linear viscoelasticity (Lee, 1955; Radok, 1957). As to the mathematical techniques to derive the concrete expressions for the viscoelastic step-response, refer to the series of papers by Matsu'ura and his co-workers (Matsu'ura et al., 1981; Sato and Matsu'ura, 1988; Matsu'ura and Sato, 1989).

3.2. Computed internal deformation fields beneath the Himalayas

Now we construct a realistic 2D plate interface model and compute the present rates of internal deformation beneath the Himalayas by using the mathematical techniques described in Section 3.1.

On the basis of the observations summarized in Section 2, we determined the geometry of the India–Eurasia plate interface as indicated by the solid line in Fig. 4. The shallow dipping plate interface (MHT) extends to the south of the MFT. The slip rates at the MHT gradually decrease to the south and vanish somewhere in the sedimentary layer of the Ganga-Basin (Seeber et al., 1981). In computation we simply assume that the MHT, with a slip rate of 20 mm/yr, extends to 100 km south of the MFT. The elastic thickness of the lithosphere is taken to be 70 km, as an average of the estimated values, ranging from 40 to 90 km (Lyon-Caen and Molnar, 1983, 1985; Jin et al., 1996; McKenzie and Fairhead, 1997; Cattin et al., 2001). Values of the structural parameters used for computation are listed in Table 1.

In Fig. 4, we show the computed internal deformation fields beneath the Himalayas due to steady slip along the India–Eurasia plate interface. The internal velocity field in Fig. 4a indicates that the steady slip along the ramp of the plate interface causes the rapid uplift of the High Himalaya. Takada and Matsu'ura (2004) have demonstrated that the computed surface uplift rates in Fig. 4a are consis-

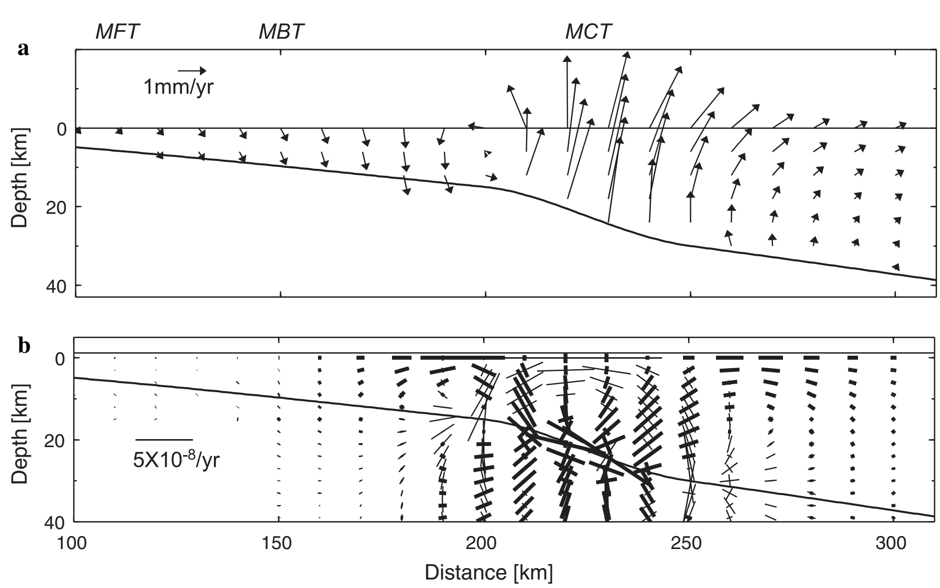

Fig. 4. Internal deformation fields beneath the Himalayas obtained by numerical simulation. (a) The internal velocity field in the coordinate system fixed to the Eurasian plate. The solid arrows indicate the velocity vectors. (b) The internal strain rates. The thick and thin bars indicate contraction and extension, respectively. In each diagram, thick line indicates the plate interface.

Table 1
Structural parameters used for the numerical simulations

	Thickness (km)	Bulk modulus (GPa)	Rigidity (GPa)	Density (kg/m^3)	Viscosity (Pa s)
Lithosphere	H	40	43	2700	∞
Asthenosphere	∞	122	67	3300	5×10^{18}

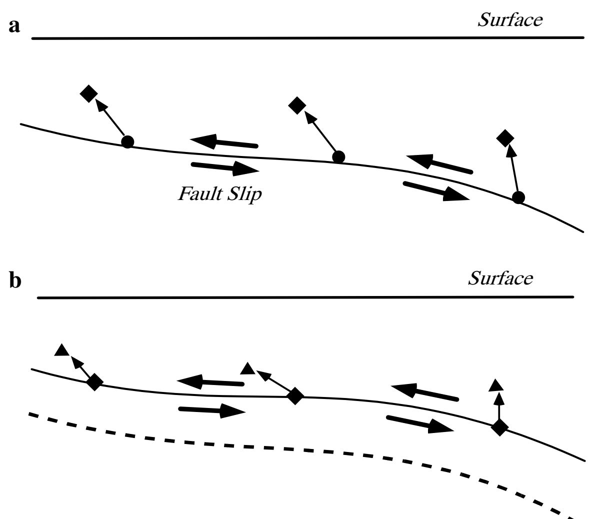

Fig. 5. A schematic diagram explaining the feedback algorithm for computing the geometric change of a fault. The solid line indicates the fault surface at each time step. A pair of thick arrows indicates the fault slip. The thin arrows indicate the computed displacement vectors for a small time interval. (a) The first procedure of the algorithm. The circles and diamonds indicate the positions of the discrete points on the upper fault surface at an arbitrary time t and at the next time step $t + \Delta t$, respectively. (b) The second procedure. The diamonds and triangles indicate the positions of the discrete points on the upper fault surface at the time and the next time step $t + 2\Delta t$, respectively. The broken line indicates the fault surface at the previous time step.

tent with the long-term uplift rates estimated from river terraces heights and levelling data. The good agreement of the computed results with observations indicates the validity of our plate convergence model. From Fig. 4b, we can see that the steady slip along the plate interface brings about remarkable strain accumulation around the ramp. On the other hand, strain changes around the flats at the left and the right of the ramp are not so remarkable, since the curvature of the plate interface is quite small there. Here, it should be noted that uniform slip along a flat interface does not cause any deformation, but the uniform slip along the curved interface causes internal deformation with an amplitude roughly proportional to its curvature.

4. Geometrical evolution of the plate interface–branch fault system

As demonstrated in Section 3.2, the internal deformation fields are directly governed by the plate interface geometry. Since the plate interface is embedded in an elastic medium, the deformation of the surrounding medium inevitably causes a geometrical change in the plate interface. This feedback mechanism is essential for understanding the geometrical evolution of the plate interface–branch fault system.

4.1. Feedback algorithm for the geometrical change of faults

In Fig. 5, we illustrate the feedback algorithm for computing the geometrical change of a fault. First, at an arbitrary time t, we compute the displacement vectors caused by a small amount of fault slip for a time interval Δt for the points arranged on the upper surface of a fault. Adding the computed displacement vectors to the position vectors of the corresponding points, we can obtain the new geometry of the fault surface at the next time step $t + \Delta t$ as shown in Fig. 5a. Then we compute the displacement vectors again for the points arranged on the new fault surface to determine the geometry of the fault surface at the subsequent time step $t + 2\Delta t$ as shown in Fig. 5b. Iterating this procedure, we can numerically simulate the geometric evolution process of the fault surface. In practice we use an interpolation technique at each step to construct a sufficiently smooth fault surface from the computed discrete

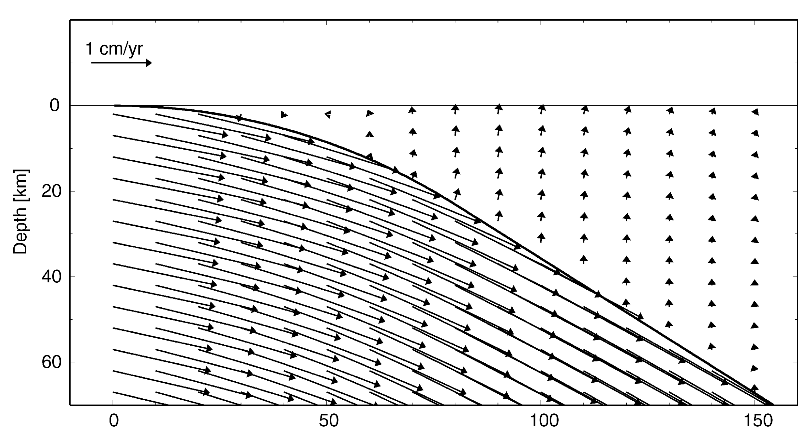

Fig. 6. Internal velocity fields due to the steady slip along the smooth plate interface. The coordinate system is fixed to the overriding plate. The arrows indicate the velocity vectors, and the solid line indicates the plate interface.

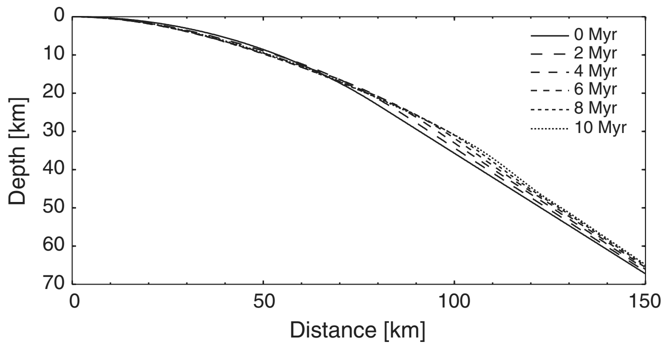

Fig. 7. Geometric change of the smooth plate interface for 10 Myr. The coordinate system is fixed to the overriding plate. The initial geometry of the plate interface is the same as that in Fig. 6.

points for saving computation time. Here, it should be noted that only the displacement components normal to the fault surface cause a change in fault geometry, because the tangential displacements represent particle motion along the fault surface.

In the following subsections, using this feedback algorithm, we numerically simulate the geometric evolution processes of the plate interface and the under-thrusting branch faults, and compute the temporal changes of crustal uplift rates to evaluate the effects of the geometric evolution of the fault system on the tectonic development of the Himalayas.

4.2. Geometrical evolution of the plate interface

First, we consider the case of a sufficiently smooth plate interface, which is represented by an arc with a small curvature in the shallower part and a straight line in the deeper part. The thickness of the lithosphere and the radius of the arc are taken to be 50 and 150 km, respectively. The arc-straight conversion point is located at 80 km on the abscissa. The steady slip rate along the plate interface is set at 20 mm/yr. In Fig. 6, we show the computed internal velocity fields in the coordinate system fixed to the overriding plate. We can see that steady subduction of the underlying plate is realized. The steady uplift motions in the overriding plate are very weak. Fig. 7 shows the geometric change of the plate interface for 10 Myr. From this figure, we can see that the geometry of the plate interface does not significantly change for 10 Myr. The reason is that the displacement components normal to the fault surface are everywhere small, as shown in Fig. 6. In short, when the plate interface is sufficiently smooth, its geometry does not significantly change on a geological time scale.

Next, we consider the case of a plate interface with a ramp. The thickness of the lithosphere is taken to be 70 km. Given the present geometry of the plate interface beneath the Himalayas (Fig. 4) and the 20 mm/yr steady back slip (normal slip), we traced the geometric evolution process of the plate interface for the last 4 Myr. Unlike the other two cases, we computed the geometry of the plate interface at each time step from the present to the past, by which we can obtain the same result as that obtained by the simulation from the past to the present. Through this retrograde simulation we can simulate the geometric evolution of the plate interface from 4 million years before the present (Myr BP) to the present day (Fig. 8). In Fig. 8, we can find that the offset of the ramp, which stands for the difference in depth across the entire ramp, decreases with time and the ramp structure migrates towards the hanging-wall side at the rate of $v_{pl}/2$ (10 mm/yr).

The internal velocity fields in Fig. 4a indicate a weak subsidence over the flat in the southern continuation of the ramp and a weak uplift over the flat of northern continuation. This deformation pattern causes a reduction in offset of the ramp. If the underlying plate does not deform, the ramp must migrate towards the hanging-wall side at the rate of v_{pl} (20 mm/yr). In fact, as shown in Fig. 4b, the strain rates of the underlying plate are the almost same as those of the overriding plate. This is the reason why the ramp migrates to the hanging-wall side at the rate of $v_{pl}/2$.

As a result of geometrical evolution of the plate interface, the pattern of surface uplift rates changes with time, as shown in Fig. 9. From this figure, we can find that the uplift pattern also migrates towards the hanging-wall side at the rate of $v_{pl}/2$ with a decreasing amplitude. Integrating these uplift rates over a time, we can obtain the total amount of uplift for the corresponding period. Fig. 10 shows the height change associated with steady slip along the ramp during the last 4 Myr. Although the growth rate of the peak gradually decreases with time, peak height reaches about 10 km over 4 Myr. This amount of uplift is enough to form the topographic height of the present High Himalaya.

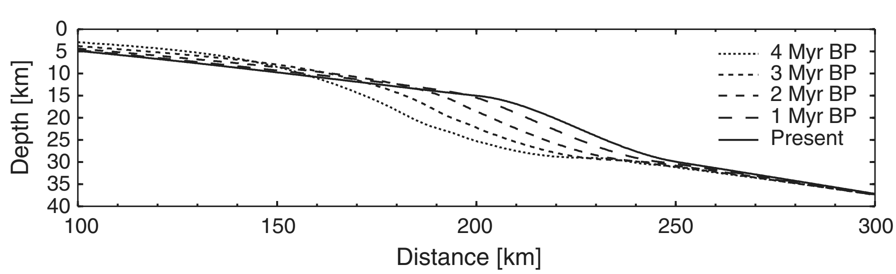

Fig. 8. Geometric change of the plate interface with a ramp beneath the High Himalaya for the last 4 Myr. The coordinate system is fixed to the overriding plate.

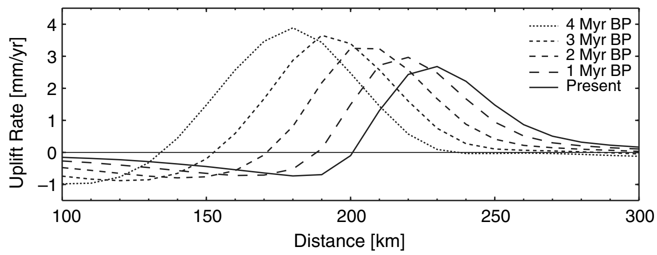

Fig. 9. Change in surface uplift rates with time, associated with the geometrical evolution of the plate interface with a ramp beneath the High Himalaya. The coordinate system is fixed to the overriding plate.

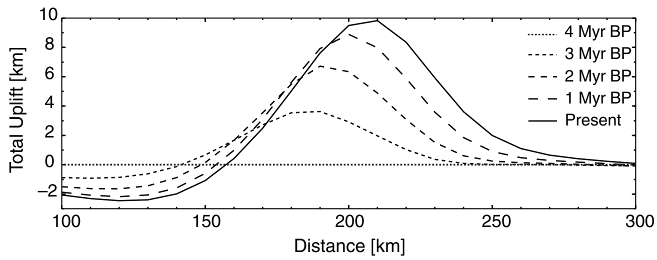

Fig. 10. Height change associated with steady slip along the ramp during the last 4 Myr. The coordinate system is fixed to the overriding plate.

4.3. Geometric evolution of the under-thrusting branch faults

In Section 4.2, we numerically simulated the process of the geometrical evolution of a plate interface with a ramp, and evaluated its effect on the tectonic development of the Himalayas. Now we consider the geometrical evolution of the under-thrusting faults branching from the plate interface.

In Himalaya the plate interface (MHT), as described in Section 2, is accompanied by a series of large-scale under-thrusting branch faults, the MCT, the MBT, and the MFT. We commence the computation of the geometrical evolution of the branch faults from the initial state shown in Fig. 11. Here, the ramp structure of the plate interface is ignored. The structural parameters of the lithosphere–asthenosphere system and the plate convergence rate are taken to be the same as in the previous cases. The depth of the branching point is set at 40 km. We take the steady slip rate at the MHT as 20 mm/yr in the portion deeper than the branching point. In the portion shallower than the branching point we assumed a steady slip rate of 10 mm/yr along both the MHT and the branch fault, that is, the total slip rate of 20 mm/yr is equally distributed between these two faults. Fig. 11 shows the internal velocity field caused by steady slip along the MHT and the branch fault in the initial state. From Fig. 11a, we can recognize the steady subduction of the underlying plate along the MHT and the nearly uniform horizontal motion of the footwall side block of the branch fault. We scaled up the velocity vectors in the hangingwall of the branch fault in Fig. 11a by five times and redrew them in Fig. 11b which clearly shows the uplift motion of the hanging-wall block.

In Fig. 12a, we show the process of geometrical evolution of the thrust fault branching from the MHT at a depth of 40 km. Here, the total amount of slip along the branch fault is used as a measure of the duration of the movement. We can summarize the characteristics of the change in the geometry of the branch fault as follows: (1) The branch fault moves towards the hanging-wall side due to the plunge of the wedge-shaped block on the footwall side. (2) The angle of dip of the branch fault increases at an increasing rate with time. Since the rate of the increase in the angle of dip becomes less with increasing depth, fault curvature increases with time. (3) The plate interface around the branching point is uplifted and a ramp structure is developed with time. This means that steady slip along the branch fault produces a new source of deformation along the plate interface.

In Fig. 12b, we show the process of geometrical evolution of the thrust fault branching from the MHT at a depth of 20 km. Here, the dip of the fault at the surface is taken to be the same as in the previous case. The characteristics of the change in geometry for a shallow branch fault are essentially the same as those for a deep branch fault, except for the increase rate of the dip-angle. That is, the rate of increase in the dip-angle of a shallow branch fault is about twice as high as that for a deep branch fault.

The mechanism of the geometrical change of branch faults is illustrated in Fig. 13, where thick arrows represent the displacement vectors on the upper surface of a branch fault in a coordinate system fixed to the hanging-wall block. As mentioned in Section 4.1, the change in fault geometry is caused by the spatial differences in the displacement components normal to the fault surface. In the present case, since fault dip increases with decreasing depth, the fault-normal displacement components take larger values in the shallower portion of the fault as illustrated in Fig. 13. Such a mechanism inevitably makes the branch fault geometry more and more listric with time.

As for the difference in the increased rate of change in dip-angle between a shallow branch fault and a deep branch fault, we can interpret this as follows: let's consider the change in the geometry of two thrust faults with the same dip, but different branching depths, as shown in Fig. 14. If the slip rates of these branch faults are the same, the fault-normal displacement components at the surface are also the same. Here, we denote the projection of the normal components on the surface by ΔX. Then, for the shallow and the deep branch faults, ΔX are the same, but the branching depths are different, and so the increments of fault dip are different. If the branching depth of the deep branch fault is twice as large as that of the shallow branch fault, the increment of fault dip of the deep branch fault is about a half of that of the shallow branch fault (Fig. 14). That is, the increase rate of fault dip is roughly proportional to the inverse of the branching depth.

The accelerative increase in fault dip will lead to a reduction in the slip rate along the branch faults and result in the cessation of movement along them, since steeply dipping branch faults cannot accommodate effectively the horizontal convergence between the two blocks. The cessation of steady slip along a branch fault means that its tectonic development also ceases. However, after the cessation of steady slip along a branch fault, another branch fault with a shallow dip will be activated to accommodate the horizontal convergence. Here, it should be noted that the total amount of horizontal convergence accommodated by a shallow branch fault is much smaller than that accommodated by a deep branch fault, because the rate of increase in the dip of the fault is roughly proportional to the depth of the branching point (Fig. 14). In other words, the life of a branch thrust fault is roughly proportional to the depth of its branching point.

In Fig. 15, we show the change in crustal uplift rates associated with the geometrical evolution of the deep branch fault (Fig. 12a). Here, the horizontal distance is measured from the surface trace of the branch fault. We can find a significant change in uplift rates near the outcrop of the branch fault. To evaluate the effects of the change in the geometry of branch faults on tectonic development, we integrate the instantaneous uplift rates over the period in which the mean fault dip increases by 10°. Fig. 16 shows the integrated total uplifts for shallow (20 km) and deep (40 km) branch faults. From this figure, we can see that the total uplift caused by a deep branch fault is about twice as larger as that caused by a shallow branch fault.

5. Discussion

In the Himalaya three major thrust faults (MCT, MBT, and MFT) branch from the Indian–Eurasian plate interface (MHT) with a large-scale ramp beneath the High Himalaya. As demonstrated by Takada and Matsu'ura (2004), the present crustal movements in Himalaya can be well explained by steady slip along the MHT and MBT. To understand the long-term tectonic development of the Himalaya, however, we must consider the geometrical evolution of the fault system as a feedback process of internal deformation and geometric fault change. Based on this idea we have simulated numerically the processes of the geometrical evolution of the plate interface (MHT) and the branch thrust faults (MCT and MBT), and have demonstrated the fundamental mechanisms of the evolution of the geometry of a plate interface–branch fault system. Through the computation of the cumulative crustal uplifts associated with the geometric evolution of the fault system, we also evaluated the effects of the change in fault geometry on tectonic development. In the following part of this section, by combining these simulation results with geological evidence summarized in Section 2, we propose a scenario of the tectonic development of the Himalayas for the last 30 Myr.

The process of the tectonic development of the Himalayas can be divided roughly into the three stages as shown in Fig. 17. In the first stage the main tectonic event is the start of active thrust motion on the MCT, schematically shown in Fig. 17a. Active thrust motion on the MCT during a period from 30 to 15 Myr BP caused a large amount of crustal uplift on the hanging-wall side. Since the branching point is deep, the increase rate in fault dip of the MCT must have been quite slow. This is consistent with the long duration of the MCT activity and the large amount of total convergence accommodated by the MCT (e.g. Schelling and Arita, 1991; Schelling, 1992). The large amount of slip along the MCT with a deep branching point must have effectively

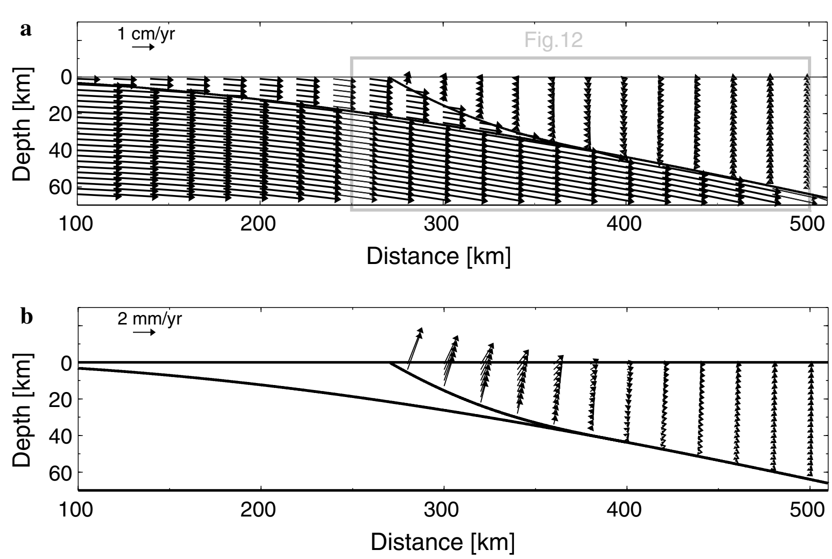

Fig. 11. Internal velocity field caused by the steady slip along the MHT and the branch fault. The coordinate system is fixed to the overriding plate. The arrows indicate the velocity vectors. The solid lines indicate the fault surfaces. The depth of the branching point is taken to be 40 km. The slip rate along the MHT is taken to be 20 mm/yr in the portion deeper than the branching point. In the shallower portion the toal slip rate (20 mm/yr) is equally distributed to the MHT and the branch fault. (a) Entire velocity field. (b) The internal velocity field in the hangingwall of the branch fault. The velocity vectors in (a) are scaled up by five times.

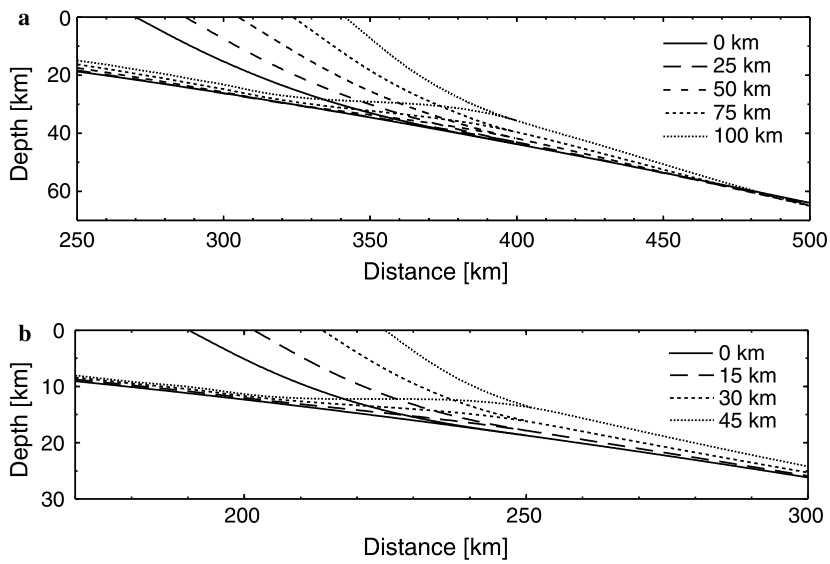

Fig. 12. Geometrical evolution of the thrust fault branching from the MHT. The total amount of slip along the branch fault is used as a measure of the duration time. (a) The case of the deep thrust fault with the branching point at 40 km depth. (b) The case of the shallow thrust fault with the branching point at 20 km depth.

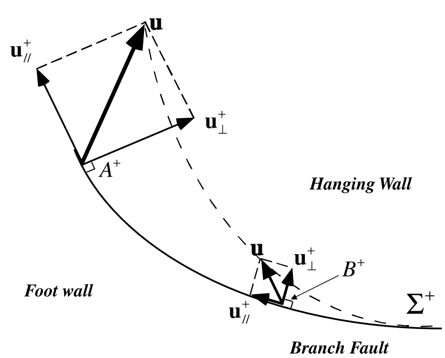

Fig. 13. A schematic diagram explaining the mechanism of the geometric change of a branch fault. A^+ and B^+ are the points on the upper surface of the branch fault (Σ^+). The displacement vector U is decomposed into the fault-normal and fault-parallel components, indicated by $\mathbf{u}_\perp^+$ and $\mathbf{u}_{//}^+$, respectively. The coordinate system is fixed to the hanging wall. The solid line indicates the surface of the branch fault. The broken line indicates the new fault surface. The left side of the solid line corresponds to the wedge between the branch fault and the MHT.

transported rocks from depth to the earth's surface to form a high mountain range. An increase in the altitude of a mountain range is always accompanied by rapid erosion (e.g. Pinet and Souriau, 1988). Thus, the transportation of rocks from a depth and rapid surface erosion lead to a rapid exhumation of deep rocks. Actually the present hanging-wall of the MCT consists of highly metamorphosed rocks, resulting from a large amount of exhumation (e.g. LeFort, 1975; Stöcklin, 1980). As illustrated in Fig. 17a, the total amount of exhumation is greater near the outcrop of the MCT, since the total amount of uplift is the greater near the outcrop of branch faults (Fig. 16). In the High Himalaya bounded by the MCT to the south, the metamorphic grade increases from north to the south, which is in accord with the total uplift pattern shown by our simulation (Fig. 16), showing a gradual southward (left in Fig. 16) increase in the uplift of the hanging wall of the branch fault. At the end of the first stage (about 15 Myr BP) the dip of the MCT must have become so steep that horizontal convergence could not be accommodated effectively.

The main tectonic event in the second stage is the start of active thrust motion on the MBT, shown schematically in Fig. 17b. After the cessation of active thrust motion on the MCT, the MBT became activated from about 10 Myr BP. The slip along the MBT must have caused crustal uplift and the development of a mountain range on its hanging-wall side. On the other hand, the mountain range formed by the MCT activity would have been reduced gradually in altitude by erosion in this stage. The total amount of horizontal convergence accommodated by the MBT will be smaller than that accommodated by the MCT, because the MBT is shallower than the MCT (Schelling and Arita, 1991; Schelling, 1992). Therefore, the MBT has no ability to form a large-scale mountain range unlike the MCT (Fig. 16). Actually, as shown in Fig. 18, the mountain range formed by the MBT is of moderate height (Mahabharat Range). At present the fault dip of the MBT has become steep (Schelling and Arita, 1991; Schelling, 1992; Mugnier et al., 1994), and thrust motion along the MBT has almost stopped (Nakata et al., 1990; Mugnier et al., 1994). The cessation of surface uplift and a reduction in mountain height by erosion will follow the cessation of active thrust motion on the MBT.

The main tectonic processes in the third stage are the flattening by erosion of the old Himalaya, produced by movement along the MCT, and the uplift of the present High Himalaya due to the steady slip along the ramp of

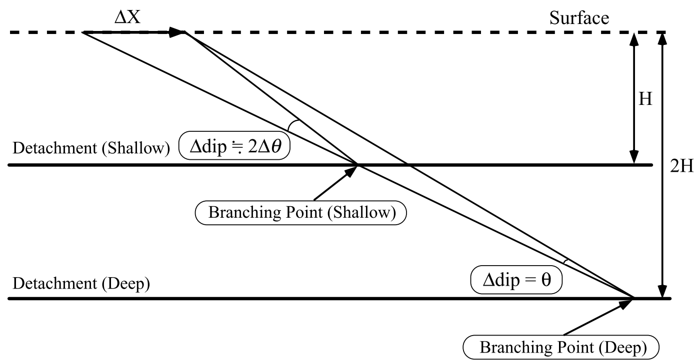

Fig. 14. Schematic diagram explaining the difference in the increase rate of dip-angle between a shallow branch fault and a deep branch fault. The thick arrow with the length of ΔX indicates the projection of the normal component $\mathbf{u}_{\perp}$ on the earth's surface. The increment in fault dip of the deep branch fault is denoted as θ.

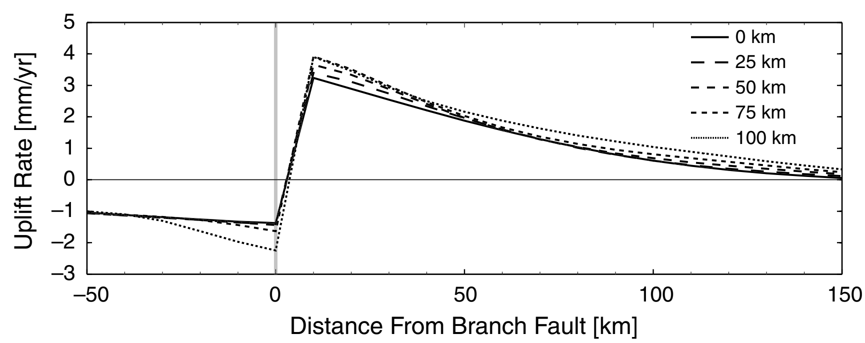

Fig. 15. Change in crustal uplift rates associated with the geometric evolution of the deep branch fault in Fig. 12a. The horizontal distance is measured from the surface trace of the branch fault. The total amount of slip along the branch fault is used as a measure of the duration time. The grey cursor line indicates the position of the branch fault.

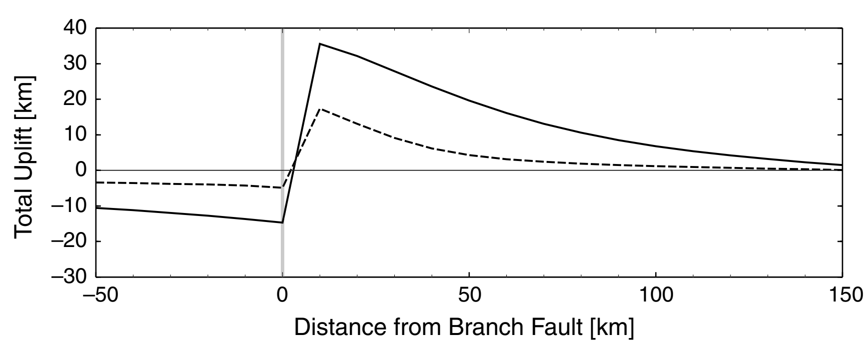

Fig. 16. Integrated total uplifts for shallow and deep branch faults. The solid and the broken lines indicate the total uplift for the deep (40 km) and the shallow (20 km) branch faults. The 0 km point of the horizontal axis, indicated by a grey cursor line, corresponds to the outcrop of the branch faults in both cases.

the plate interface, schematically shown in Fig. 17c. The altitude of the mountain range formed by movement on the MCT has been reduced by surface erosion over the past 10 Myr. At present the peak height and the mean altitude of the High Himalaya are 8000 and 5500 m, respectively (Fig. 18). It is impossible to maintain such a high mountain range for 15 Myr unless rapid crustal uplift occurs for some reason after the cessation of active thrust motion on the MCT. As demonstrated in Fig. 10, the steady slip at 20 mm/yr along a ramp in the plate interface can produce about 10 km crustal uplift over a period of 4 Myr. Based on this numerical result, we conclude that the present High Himalaya has been formed in the last several million years by the uplift of a plateau, formed by the erosion of the MCT-origin old Himalayas, due to the steady slip along the ramp of the plate interface. Finally, another branch thrust fault, the MFT, has developed recently in the sedimentary layers of the Ganga Basin to form the Siwalik Hills, marking the deformation front of the Himalaya (Fig. 18).

This scenario, based on the kinematic plate convergence model, explains well the general features of the process of

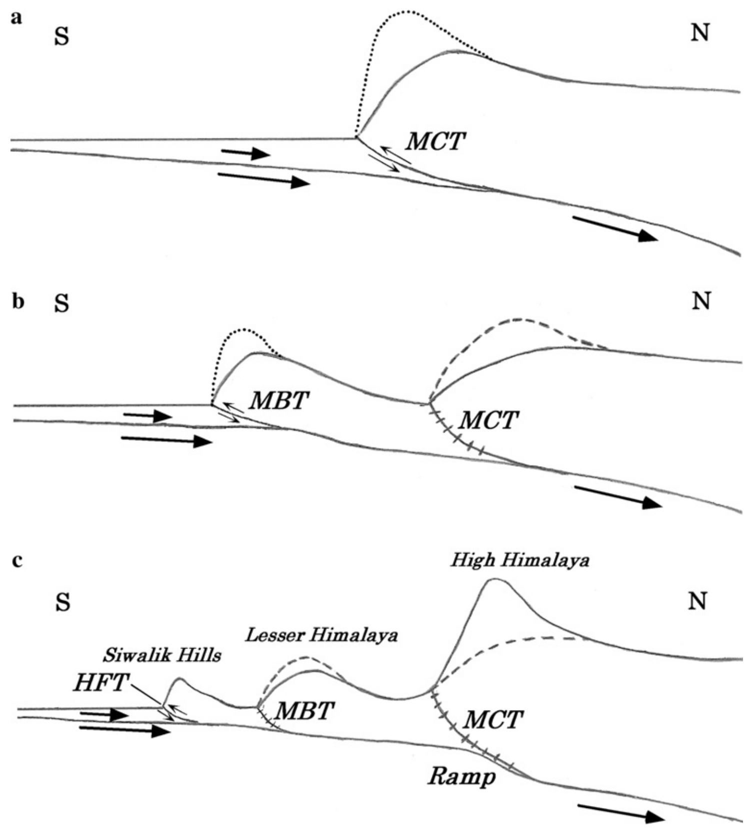

Fig. 17. A scenario of the tectonic development in the Himalayas for the last 30 Myr. The thick arrows indicate the velocity vectors relative to a stable point of the Eurasian plate. The pairs of thin arrows along the branch faults indicate active thrust motion on the fault. Staples across the branch fault indicate the cessation of thrust motion. Solid lines represent the surface topography at each moment. (a) First stage (30–15 Myr BP). The dotted line above the MCT indicates the total surface uplift caused by the slip along the MCT. (b) Second stage (10–4 Myr BP). The dotted line above the MBT indicates the total surface uplift caused by the slip along the MBT. The broken line above the MCT indicates the surface topography at the first stage. (c) Third stage (4 Myr BP–present). The broken line at the High Himalaya indicates the surface topography before the initiation of the uplift motion due to steady slip along the ramp. The broken line at the Lesser Himalaya indicates the surface topography at the second stage.

tectonic development in the Himalaya, but there still remain some problems, such as the processes for the generation of ramp structures and branch thrust faults to be solved in the future. In order to solve these problems we need to incorporate a fracture criterion of rocks into the kinematic model developed here.

6. Conclusions

Crustal deformation due to fault slip strongly depends on fault geometry and fault geometry is changed by crustal deformation. By considering such a feedback process, we have developed a kinematic model for the geometrical evolution of the plate interface–branch fault system on the basis of elastic–viscoelastic dislocation theory, and have determined the fundamental properties and mechanisms of changes in the geometry of thrust faults through numerical simulations. For the geometric change of plate interfaces, if the plate interface is smooth, no significant change will occur in fault geometry. If the plate interface has a ramp, we can observe the gradual horizontal motion of the ramp toward the hanging-wall side at half the rate of plate convergence. The offset of the ramp decreases with time. For geometrical change in thrust faults branching from the plate interface, in general, the dip-angle of the branch fault increases faster as the fault dip increases. The shallower the branching point depth, the faster the rate at which fault dip increases. Since it is more difficult for a branch fault with a steeper dip-angle to take up the horizontal convergence, the increase in fault dip results in the cessation of branch fault activity. This means that a thrust fault with a shallow branching point cannot produce large-scale mountains.

By combining the results of this simulation with geological evidence, we have proposed a scenario for the tectonic development of the Himalayas for the last 30 Myr. The process of tectonic development may be divided roughly into three stages. From 30 to 15 Myr BP, active thrust motion on the Main Central Thrust (MCT) developed a very high mountain range. After the cessation of the MCT activity, this high mountain range was gradually eroded. After 10 Myr BP the Main Boundary Thrust (MBT) became active, and developed a medium-sized mountain range. For the last several million years, steady slip along the ramp of the plate interface has raised the present High Himalaya in the same area where the old Himalaya, formed by movement along the MCT, was once located.

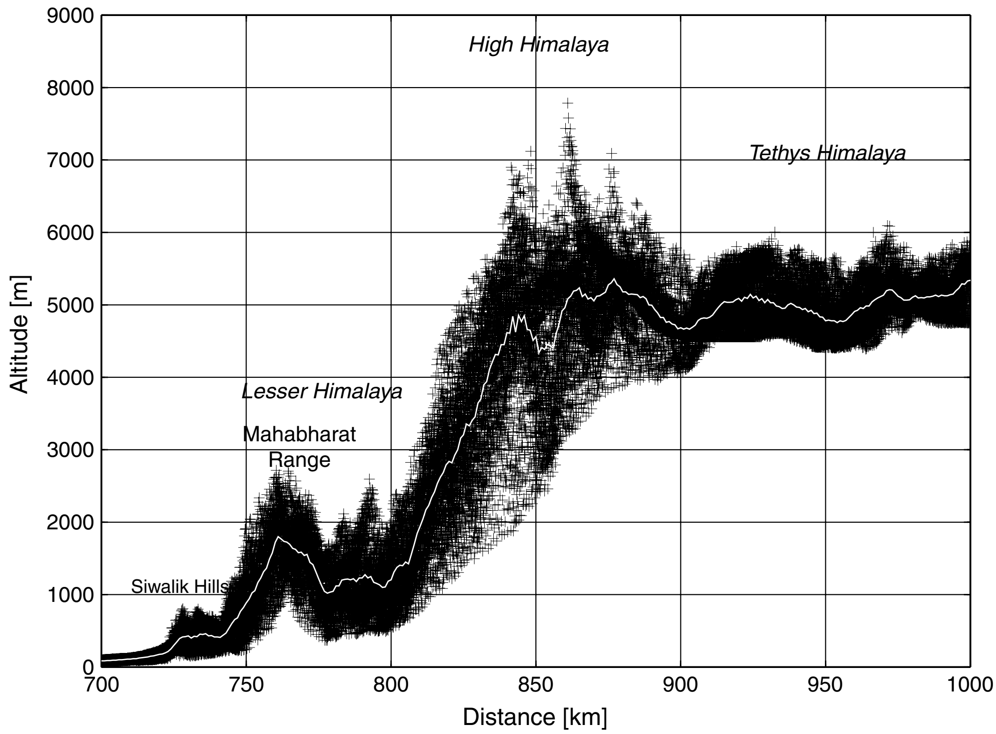

Fig. 18. The topographic profile obtained by projecting digital elevation data (U.S. Geological Survey, 1996—GTOPO30) onto a vertical plane across the Himalayan arc at Kathmandu. The crosses indicate elevation data in an area extending 50 km on each side of the arc normal line. The white line indicates the profile of the mean elevation.

Acknowledgements

We acknowledge Kazunori Arita for his helpful comments on the geologic evolution of the Himalayas. We thank John Rundle and an anonymous reviewer for thoughtful reviews. This study was supported by the Grant-in-Aid for Scientific Research from JSPS to YT.

References

Baranowski, J., Armbruster, J., Seeber, L., Molnar, P., 1984. Focal depths and fault plane solutions of earthquakes and active tectonics of the Himalaya. Journal of Geophysical Research 89, 6918–6928.

Bilham, R., Larson, K., Freymueller, J., Project LdyLhim members, 1997. GPS measurements of present-day convergence across the Nepal Himalaya. Nature 386, 61–64.

Brown, L.D., Zhao, W., Nelson, K.D., Hauck, M., Alsdorf, D., Ross, A., Cogan, M., Clark, M., Liu, X., Che, J., 1996. Bright spots, structure and magmatism in southern Tibet from INDEPTH seismic reflection profiling. Science 274, 1688–1690.

Burridge, R., Knopoff, L., 1964. Body force equivalents for seismic dislocations. Bulletin of the Seismological Society of America 54, 1875–1888.

Cathles, L.M., 1975. The Viscosity of the Earth's Mantle. Princeton University Press, Princeton, NJ.

Cattin, R., Martelet, G., Henry, P., Avouac, J.P., Diament, M., Shakya, T.R., 2001. Gravity anomalies, crustal structure and thermo-mechanical support of the Himalayas of Central Nepal. Geophysical Journal International 147, 381–392.

Chemenda, A.I., Mattauer, M., Malavieille, J., Bokun, A.N., 1995. A mechanism for syn-collisional rock exhumation and associated normal faulting: results from physical modelling. Earth and Planetary Science Letters 132, 225–232.

Chemenda, A.I., Mattauer, M., Bokun, A.N., 1996. Continental subduction and a mechanism for exhumation of high-pressure metamorphic rocks: new modelling and field data from Oman. Earth and Planetary Science Letters 143, 173–182.

Chemenda, A.I., Burg, J.P., Mattauer, M., 2000. Evolutionary model of the Himalaya–Tibet system: geopoem based on new modelling, geological and geophysical data. Earth and Planetary Science Letters 174, 397–409.

Davis, D., Suppe, J., Dahlen, F.A., 1983. Mechanics of fold-and-thrust belts and accretionary wedges. Journal of Geophysical Research 88, 1153–1172.

DeCelles, P.G., Robinson, D.M., Quade, J., Ojha, T.P., Garzione, C.N., Copeland, P., Upreti, B.N., 2001. Stratigraphy, structure, and tectonic evolution of the Himalayan fold-thrust belt in western Nepal. Tectonics 20, 487–509.

DeMets, C., Gordon, R.G., Argus, D.F., Stein, S., 1990. Current plate motions. Geophysical Journal International 101, 425–478.

England, P., Molnar, P., 1997. The field of crustal velocity in Asia calculated from Quaternary rates of slip on faults. Geophysical Journal International 130, 551–582.

Friedenreich, O.R., Slind, O.L., Pradhan, U.M.S., Shrestha, R.B., 1994. Petroleum geology of Nepal. Canadian Journal of Exploration Geophysics 30, 103–114.

Fukahata, Y., Matsu'ura, M., 2005. General expressions of internal deformation fields due to a dislocation source in a multilayered elastic half-space. Geophysical Journal International 161, 507–521.

Gansser, A., 1964. Geology of the Himalayas. Wiley–Interscience, London.

Gansser, A., 1981. The geodynamic history of the Himalaya. In: Gupta, H.K., Delany, F.M. (Eds.), Zagros, Hindu Kush, Himalaya, Geodynamic Evolution, Geodynamics Series 3. American Geophysical Union, Washington, DC, pp. 111–121.

Harrison, T.M., Copeland, P., Kidd, W.S.F., Yin, A., 1992. Raising Tibet. Science 255, 1663–1670.

Hodges, K.V., 2000. Tectonics of the Himalaya and southern Tibet from two perspectives. Geological Society of America Bulletin 112, 324–350.

Hodges, K.V., Hubbard, M.S., Silverberg, D.S., 1988. Metamorphic constraints on the thermal evolution of the central Himalayan orogen. Philosophical Transactions of the Royal Society, London A 326, 257–280.

Iwasaki, T., Matsu'ura, M., 1982. Quasi-static crustal deformations due to a surface load: rheological structure of the earth's crust and upper mantle. Journal of the Physics of the Earth 30, 469–508.

Iwata, S., Sharma, T., Yamanaka, H., 1984. A preliminary report on geomorphology of central Nepal and Himalayan uplift. Journal of Nepal Geological Society 4, 141–149.

Jackson, M., Bilham, R., 1994. Constraints on Himalayan deformation inferred from vertical velocity fields in Nepal and Tibet. Journal of Geophysical Research 99, 13897–13912.

Jin, Y., McNutt, M.K., Zhu, Y., 1996. Mapping the descent of Indian and Eurasian plates beneath the Tibetan Plateau from gravity anomalies. Journal of Geophysical Research 101, 11275–11290.

Kono, M., 1974. Gravity anomalies in east Nepal and their implications to the crustal structure of the Himalayas. Geophysical Journal of the Royal Astronomical Society 39, 283–299.

Larson, K.M., Bürgmann, R., Bilham, R., Freymueller, J., 1999. Kinematics of the India–Eurasia collision zone from GPS measurements. Journal of Geophysical Research 104, 1077–1094.

Lavé, J., Avouac, J.P., 2000. Active folding of fluvial terraces across the Siwalik Hills, Himalayas of central Nepal. Journal of Geophysical Research 105, 5735–5770.

Lee, E.H., 1955. Stress analysis in visco-elastic bodies. Quarterly of Applied Mathematics 13, 183–190.

LeFort, P., 1975. Himalayas: the collided range. Present knowledge of the continental arc. American Journal of Science 275-A, 1–44.

LeFort, P., 1986. Metamorphism and magmatism during the Himalayan collision. In: Coward, M.P., Ries, A.C. (Eds.), Collision Tectonics, Geological Society of London Special Publication 19. Blackwell Scientific Publications, Oxford, pp. 159–172.

Lyon-Caen, H., Molnar, P., 1983. Constraints on the structure of the Himalaya from an analysis of gravity anomalies and a flexural model of the lithosphere. Journal of Geophysical Research 88, 8171–8191.

Lyon-Caen, H., Molnar, P., 1985. Gravity anomalies, flexure of the Indian plate, and the structure, support and evolution of the Himalaya and Ganga Basin. Tectonics 4, 513–538.

Maruyama, T., 1963. On the force equivalents of dynamical elastic dislocations with reference to the earthquake mechanism. Bulletin of the Earthquake Research Institute, University of Tokyo 41, 467–486.

Matsu'ura, M., Sato, T., 1989. A dislocation model for the earthquake cycle at convergent plate boundaries. Geophysical Journal International 96, 23–32.

Matsu'ura, M., Tanimoto, T., Iwasaki, T., 1981. Quasi-static displacements due to faulting in a layered half-space with an intervenient viscoelastic layer. Journal of the Physics of the Earth 29, 23–54.

McKenzie, D., Fairhead, D., 1997. Estimates of the effective elastic thickness of the continental lithosphere from Bouguer and free air gravity anomalies. Journal of Geophysical Research 102, 27,523–27,552.

Meigs, A.J., Burbank, D.W., Beck, R.A., 1995. Middle-late Miocene (greater-than-10 Ma) formation of the main boundary thrust in the western Himalaya. Geology 23, 423–426.

Molnar, P., 1984. Structure and tectonics of the Himalaya: constraints and implications of geophysical data. Annual Review of Earth and Planetary Sciences 12, 489–518.

Molnar, P., 1987. Inversion of profiles of uplift rates for the geometry of dip-slip faults at depth, with examples from the Alps and the Himalaya. Annales Geophysicae 5, 663–670.

Molnar, P., Tapponnier, P., 1975. Cenozoic tectonics of Asia: effects of a continental collision. Science 189, 419–426.

Mugnier, J.L., Huyghe, P., Chalaron, E., Mascle, G., 1994. Recent movements along the Main Boundary Thrust of the Himalayas: normal faulting in an over-critical thrust wedge? Tectonophysics 238, 199–215.

Nakata, T., Otsuki, K., Khan, S.H., 1990. Active faults, stress field, and plate motion along the Indo-Eurasian plate boundary. Tectonophysics 181, 83–95.

Nelson, K.D. et al., 1996. Partially molten middle crust beneath southern Tibet: synthesis of project INDEPTH results. Science 274, 1684–1688.

Ni, J., Barazangi, M., 1984. Seismotectonics of the Himalayan collision zone: geometry of the underthrusting Indian plate beneath the Himalaya. Journal of Geophysical Research 89, 1147–1163.

Pinet, P., Souriau, M., 1988. Continental erosion and large-scale relief. Tectonics 7, 563–582.

Powers, P.M., Lillie, R.J., Yeats, R.S., 1998. Structure and shortening of the Kangra and Dehra Dun reentrants, Sub-Himalaya, India. Geological Society of America Bulletin 110, 1010–1027.

Radok, J.R.M., 1957. Visco-elastic stress analysis. Quarterly of Applied Mathematics 15, 198–202.

Sato, R., Matsu'ura, M., 1973. Static deformations due to the fault spreading over several layers in a multi-layered medium. Part I. Displacement. Journal of the Physics of the Earth 21, 227–249.

Sato, T., Matsu'ura, M., 1988. A kinematic model for deformation of the lithosphere at subduction zones. Journal of Geophysical Research 93, 6410–6418.

Sato, T., Matsu'ura, M., 1993. A kinematic model for evolution of island arc-trench systems. Geophysical Journal International 114, 512–530.

Schelling, D., 1992. The tectonostratigraphy and structure of the eastern Nepal Himalaya. Tectonics 11, 925–943.

Schelling, D., Arita, K., 1991. Thrust tectonics, crustal shortening, and the structure of the far-eastern Nepal Himalaya. Tectonics 10, 851–862.

Seeber, L., Armbruster, J.G., Quittmeyer, R.C., 1981. Seismicity and continental subduction in the Himalayan arc. In: Gupta, H.K., Delany, F.M. (Eds.), Zagros, Hindu Kush, Himalaya, Geodynamic Evolution, Geodynamics Series 3. American Geophysical Union, Washington, DC, pp. 215–242.

Shemenda, A.I., Grocholsky, A.L., 1992. Physical modelling of lithosphere subduction in collision zones. Tectonophysics 216, 273–290.

Stöcklin, J., 1980. Geology of Nepal and its regional frame. Journal of the Geological Society, London 137, 1–34.

Takada, Y., Matsu'ura, M., 2004. A unified interpretation of vertical movement in Himalaya and horizontal deformation in Tibet on the basis of elastic and viscoelastic dislocation theory. Tectonophysics 383, 105–131.

U.S. Geological Survey, 1996. GTOPO30: Global 30 Arc Second Elevation Data Set.

Wesnousky, S.G., Kumar, S., Mohindra, R., Thakur, V.C., 1999. Uplift and convergence along the Himalayan Frontal Thrust of India. Tectonics 18, 967–976.

Willett, S., Beaumont, C., Fullsack, P., 1993. Mechanical model for the tectonics of doubly vergent compressional orogens. Geology 21, 371–374.

Zhao, W., Nelson, K.D., Project INDEPTH Team, 1993. Deep seismic reflection evidence for continental underthrusting beneath southern Tibet. Nature 366, 557–559.